—SUPPLEMENTARY INFORMATION—

PRIVATE VALUE OF MANGROVE COASTAL PROTECTION BENEFITS

TENG LIU[1], MICHAEL BECK[1], BROOK CONSTANTZ[1], BORJA REGUERO[1], DAVID GUTIÉRREZ-BARCELÓ[1], GALINA HALE[1,2*]

Contents

1 Introduction **3**

2 Data Sources and Damage Calculation Methodology **4**

2.1 Flood Risk Maps and Modeling 4

2.1.1. Flood modeling 4

2.1.2. Flood model surface 4

2.1.3. Extreme events 4

2.1.4. Ocean waves 5

2.2 Direct Damages to Infrastructure 5

2.2.1. Building data 5

2.2.2. Damage functions 5

2.2.3. Flood probability adjustment (extensive margin) 6

2.2.4. Summarization at the County-level 7

2.3 Key Model Limitations and Assumptions 7

3 Net Present Value of Housing Framework: Model and Calibration **8**

3.1 Conceptual Framework 8

3.1.1. Setup 8

3.1.2. Consumption growth with climate disasters 8

3.2 Key Parameters 9

3.2.1. Storm occurrence probabilities 10

3.2.2. Climate change scenarios 10

Date: October 3, 2026

[1]University of California, Santa Cruz, CA USA.
[2]NBER, CEPR.
*Corresponding author. gbhale@ucsc.edu.

3.2.3. Consumption shocks 11
3.2.4. Rental yield 13
3.2.5. County-specific hedonic loss parameters 16
3.2.6. Sensitivity to the return-period scaling rule 17
3.3 Comparing to hedonic measure 18
3.4 Comparison with the expected-damages valuation 19
3.5 County-level protection values 20
Appendix A Derivation of Eq. (S9) **21**
Appendix B Results obtained with structure value-weighted average loss ratio **22**
References **25**

1. Introduction

Our approach combines engineering estimates of physical flood protection with consumption-based asset pricing theory to value mangrove coastal protection. Building on prior work showing that mangroves reduce storm-surge damages ([1], [2], and [3]), we estimate building-level flood protection directly from SFINCS (Super-Fast INundation of CoastS) flood maps, generated with and without mangroves across storm return periods and climate scenarios, coupled with the Federal Emergency Management Agency (FEMA) Flood Assessment Structure Tool (FAST) and Hazus depth-damage functions (FEMA's flood loss-estimation methodology). We incorporate both intensive-margin (reduced flood depths) and extensive-margin (reduced probability of flooding) protection effects via a flood-probability adjustment to the structural damage ratio in mangrove scenarios. These engineering-based damage and probability inputs serve as inputs to our state-dependent valuation framework, generating risk-adjusted values that reflect the amplified marginal utility of protection in disaster states. Storm risk is modeled using return-period-based annual probabilities in Monte Carlo simulations, and climate-change scenarios incorporate sea level rise and associated changes in flood hazard while holding mangrove protective capacity constant. We then aggregate property-level protection values to counties using a consistent at-risk exposure base and compare these theory-based values to market valuations derived from hedonic analysis [4], providing a perspective on market efficiency.

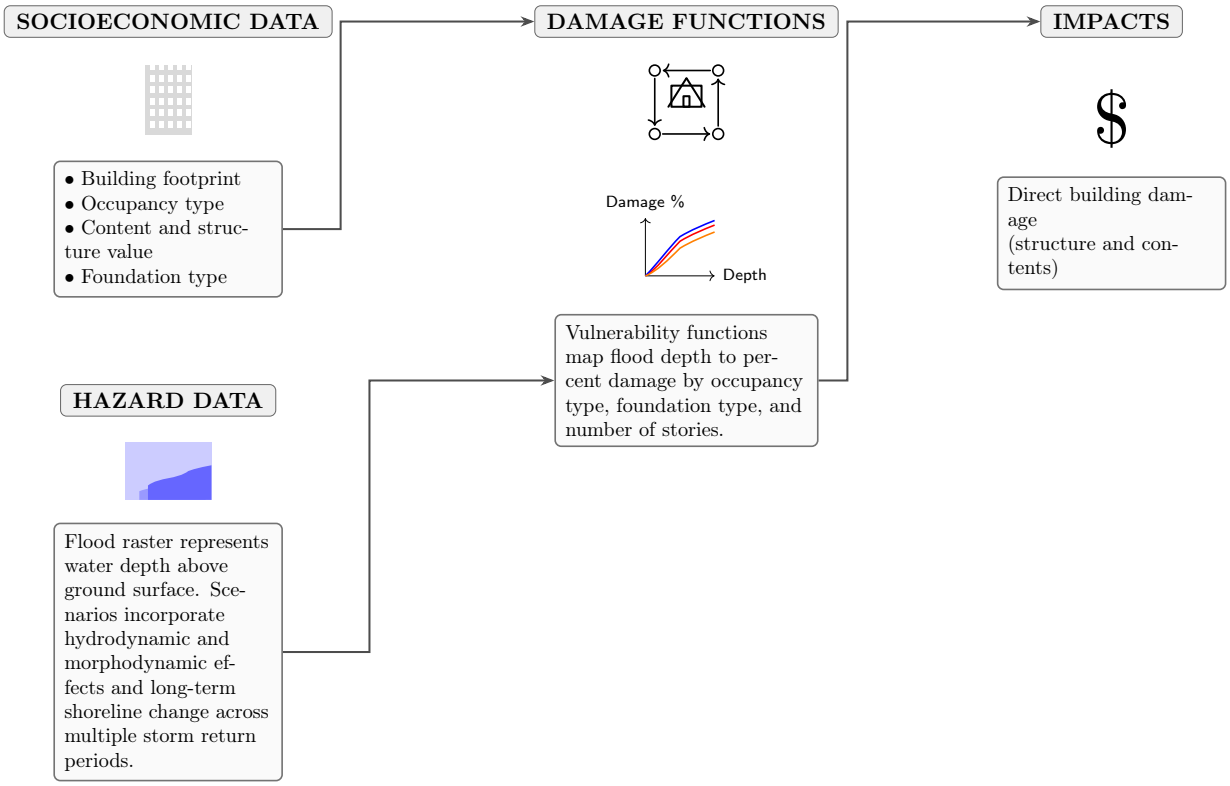


Figure S1. Flood damage assessment workflow. Building-level socioeconomic data and flood hazard maps are combined using depth–damage vulnerability functions to estimate direct economic impacts. Adapted from FEMA FAST [5].

2. Data Sources and Damage Calculation Methodology

This section describes the data sources and methods used to estimate flood damages and the flood-protection value of mangroves. We couple hydrodynamic flood modeling — which produces flood-depth maps under each mangrove and climate scenario from elevation, land-cover, and extreme sea-level and wave data — with building-level exposure data and FEMA Hazus depth–damage functions to compute direct damages for every affected structure (Figure S1) [6].

2.1. **Flood Risk Maps and Modeling.**

Our flood maps are produced by hydrodynamic modeling of current and future coastal flooding and of the flood-risk reduction provided by mangroves (Figure S1); we do *not* use FEMA flood-zone maps to determine which properties are exposed. This modeling yields a high-resolution, regional assessment of coastal flooding and the benefits of mangroves. These 10-m resolution flood maps cover two habitat scenarios (with and without mangroves), four storm return periods (10, 25, 50, 100-year) and two climate scenarios (current and future 2050s).

2.1.1. *Flood modeling.*

The SFINCS model is used to calculate flood extent and inland water depths for all the different scenarios and produce flood maps representing the maximum depth at each location during each simulated storm [7]. SFINCS is suitable for large-scale modeling as it allows high computational efficiency while maintaining adequate accuracy. The model is fed with water level time series by scaling the shape of the storm hydrograph with the local tide and the extreme water levels that result from the set-up and run-up analysis. The boundary conditions are one kilometer resolution across each region.

2.1.2. *Flood model surface.*

The surface flooded by SFINCS is created using elevation data from a composite of federal products, prioritized for each location from most to least accurate and granular. Native resolutions range from 1 m to ∼450 m: USGS 3DEP lidar [1 m, land; 8], NOAA CUDEM [∼ 3 m, nearshore topobathymetry; 9], the 2008 National Elevation Dataset [∼ 3 m, land gap fill; 10], NOAA BlueTopo [∼4–16 m, offshore; 11], and ETOPO 2022 [∼450 m, deep-offshore gap fill only; 12]. All sources are merged onto a common 10 m grid in NAD83 UTM zone 17N (EPSG:26917), using average resampling for sources finer than 10 m and bilinear interpolation for coarser sources.

The surface roughness varies spatially depending on the classification of the land cover. This classification is based on a combination of the USGS Annual National Land Cover Database (NLCD) [13] overlaid with the 2020 Global Mangrove watch data [GMW, 14]. The Manning coefficients are selected for NLCD using the land-cover lookup table of Kalyanapu et al [15]. Mangroves are given a Manning coefficient of $n = 0.14$ [16]; in the mangrove-degraded scenario, mangrove cells are instead assigned $n = 0.02$. Offshore areas beyond NLCD coverage are assigned open-water roughness ($n = 0.025$).

2.1.3. *Extreme events.*

Extreme sea level and ocean wind wave events are estimated from pre-existing datasets. For the sea level, extreme events are characterized by the maximum water level and time evolution of the storms inside each study area both in the past and in the projected future. These extreme sea level values are extracted from the COAST-RP database [17] that uses a sea level hindcast of 38 years of ECMWF Reanalysis v5 (ERA5) climate data along with the STORM dataset of synthetic tropical cyclones [18].

2.1.4. *Ocean waves.* For the ocean waves, extreme values of significant wave height are estimated and then related to wave period. These extreme values serve as inputs for the hydrodynamic models for assessing the impact of different climate scenarios on flood risk. For the ocean waves, two datasets of offshore wave conditions are used. First, an ocean wave reanalysis from the ERA5 dataset [19] covers the period between 1940 and 2023. Second, a climate change dataset produced by USGS using the latest Coordinated Model Intercomparison Project Phase 6 (CMIP6) GCMs information for historical (1979–2014) and projected (2020–2050) periods, under the SSP5-8.5 emissions scenario [20].

The shape of the evolution in time of the sea level during a storm (i.e., storm hydrograph) is determined by analyzing the extended version of the same reanalysis based on ERA5 from 1950 to 2018 [21] and following the method described by Dullaart et al. [22]. This extended dataset also contains historical (1979–2014) and projected (2020–2050) sea levels for different Global Climate Models (GCMs) under the SSP5-8.5 emissions scenario. These have been used to estimate the projected changes in extreme sea levels by 2050 (SLR and surge).

An extreme value analysis is used to determine the extreme wave events. This analysis estimates wave heights and periods for 10, 25, 50, and 100-year return periods for current sea level conditions and future conditions. The only future wave data assessed under the CMIP6 GCMs are those modeled by USGS, which assess waves to 2050 and use the SSP5-8.5 scenario as an upper bound for storm damages. However, differences in sea level and other climate metrics by mid-century among emissions scenarios are minimal [23]. Significant divergence in sea level and other ocean dynamics does not occur until late in the century. By 2050, the difference in sea level between scenarios will only be a few centimeters.

2.2. **Direct Damages to Infrastructure.** The analysis calculates flood damages at the building level by spatially joining building attributes from the National Structure Inventory (NSI) [24] with building footprint data from Microsoft Open Buildings [25]. Values in the NSI data are at 2021 price levels, and the value of structure and content is updated to 2025 prices using a cumulative price ratio of 1.19 [26].

2.2.1. *Building data.* We intersect each NSI data point with Microsoft building footprint polygons to create a model of the building landscape. Most NSI data intersect exactly one building polygon, except for some structures that are missing building footprints, and so are joined to the nearest building within 50 meters. Several NSI values are associated with a single building polygon (e.g., multi-use space or large condominiums), each sharing the same flood depth. To ensure damages are comparable across scenarios, we restrict the sample to the set of buildings flooded (depth >0) in every scenario.

2.2.2. *Damage functions.* We use the FEMA FAST tool, updated with damage functions from Hazus 7.0, to estimate flood damage types, extent, and associated economic losses [5, 6, 27, 28, 29, 30, 31]. For each building, maximum flood depth is calculated from the intersection of the flood map and the building footprint. A damage function is then selected from Hazus based on the building's combination of occupancy type, foundation type, and number of stories [6, 32, 28]. Economic damages are calculated by inputting the maximum flood depth into the corresponding damage function, yielding both percent and total damage for each structure. Hazus damage functions are provided as tabulated depth–damage relationships rather than closed-form equations: for each building type k, Hazus specifies a discrete set of pairs $\{(d_i, D_k(d_i))\}_{i=0}^{N}$ where d_i denotes flood depth relative to the first finished floor (tabulated at 1 ft intervals, typically from -2 to $+16$ ft relative to the first finished floor) and $D_k(d_i) \in [0, 100]$ is the percent structural damage. For an observed flood depth d at a given building, we estimate

damage by piecewise-linear interpolation between the two nearest tabulated depths (equation S1), implemented via `numpy.interp`. These analyses are repeated across all flood depth maps for each adaptation scenario, return interval, and climate scenario. We refer to the sum of these damages as "direct damages."

$$D_k(d) = D_k(d_i) + \frac{d - d_i}{d_{i+1} - d_i}\big[D_k(d_{i+1}) - D_k(d_i)\big], \qquad d_i \le d \le d_{i+1}, \tag{S1}$$

For each building, the percent structural damage $D_k(d)$ gives a per-structure loss ratio (damage as a share of total building value). We average these ratios, unweighted, across all buildings flooded in each county, return period, and scenario to obtain the county-level direct loss parameter ξ_h shown in Figure S2.

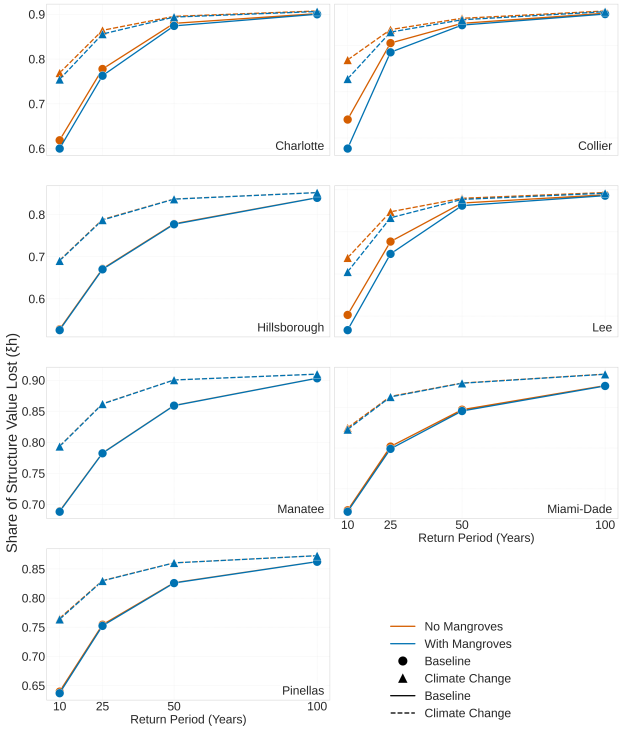


FIGURE S2. **Direct loss parameter.** Unweighted average share of building value lost (ξ_h) among buildings affected by flooding, by county, return period, and scenario. Values are the raw (unadjusted) damage ratios; the flood-probability adjustment is applied downstream. The structure value-weighted version is reported in Appendix B.

2.2.3. *Flood probability adjustment (extensive margin).* To reflect that mangroves can reduce not only flood depths (intensive margin) but also the likelihood that a property floods at all (extensive margin), we apply a flood-probability adjustment to the structural damage ratio ξ_h in scenarios where mangroves are present. For each county–return period–climate scenario, we compute a flood probability factor as the ratio of the number of flooded buildings (depth $>$ 0) in the "with mangroves" scenario to the number of flooded buildings in the corresponding "without mangroves" scenario, N^m_{flood}/N^0_{flood}. We then scale the mangrove damage ratio by this factor, $\xi_h^{m,adj} = \min\{1, \xi_h^m \cdot (N^m_{flood}/N^0_{flood})\}$.

2.2.4. *Summarization at the County-level.* We summarized all damages and building value attributes at the county-level to focus on overall trends. All building data was assigned a county by intersecting their locations with county boundaries for the seven counties in this study [33]. Summarizing at the county level allowed us to simultaneously evaluate the benefits of mangroves to building-level direct-damage protection and to housing sale price impacts [4].

2.3. **Key Model Limitations and Assumptions.** All regional and global flood models have limitations and are heavily influenced by available data particularly on elevation, bathymetry and economic assets. The digital elevation model used in this analysis is a composite of federal elevation products resampled to a 10-meter grid. Despite adjustments, "noise" from land features such as trees and buildings can be misidentified as base elevation, which can inflate the actual terrain height, creating artificial barriers that lead to an underestimation of flooded areas. To mitigate this in mangrove-covered regions, elevations above mean sea level (MSL) were manually reset to MSL.

Even high-resolution elevation data typically do not capture local flood defenses like seawalls or dikes. This is a common challenge not only for global models but also for high-resolution industry models used in highly developed areas such as Florida, USA. When there are no data on existing defenses, models tend to overestimate flooding. Consequently, future analyses would benefit from updated bathymetry, explicit representation of coastal defense structures, and refined economic asset data.

3. Net Present Value of Housing Framework: Model and Calibration

This section describes the asset-pricing framework used to value housing as the discounted present value of future housing services and to quantify how climate-driven flood risk affects those cash flows. We first establish the household optimization problem with Constant Relative Risk Aversion (CRRA) utility and derive the stochastic discount factor (pricing kernel) that reflects households' elevated marginal utility during consumption shocks. We then use this discount factor to derive the housing price equation under disaster risk, which incorporates both flood-induced consumption shocks (ξ_c) and structural housing damages (ξ_h). We then describe how we simulate disaster arrivals and calibrate key parameters used to map physical flood scenarios into net present value impacts.

3.1. **Conceptual Framework.**

3.1.1. *Setup.* **Preferences:** Representative household with CRRA utility:

$$U(c_t) = \frac{c_t^{1-\gamma}}{1-\gamma} \tag{S2}$$

where γ is the coefficient of relative risk aversion

Consumption:

$$c_t = y_t + d_t \tag{S3}$$

where y_t is non-housing consumption and d_t are housing services/consumption.

3.1.2. *Consumption growth with climate disasters.* Following the literature on consumption-based asset pricing and rare disasters [34, 35, 36, 37], we decompose consumption growth into normal and disaster states s_t:

$$s_t = \begin{cases} 0 & \text{no disaster} \\ 1 & \text{disaster} \end{cases}$$

with

$$\mathbb{P}_t(s_t = 1) = p_t$$

$$\mathbb{E}_t\left[\frac{c_{t+1}}{c_t}\right] = (1+g_c)(1-p_{t+1}\,\xi_c) \tag{S4}$$

where ξ_c is the consumption impact of the hurricane disaster.

Assuming CRRA utility function with risk aversion coefficient γ and discount rate β, the stochastic discount factor is time-varying and state-dependent:

$$m_{t+1} = \beta\left(\frac{c_{t+1}}{c_t}\right)^{-\gamma}(1-s_{t+1}\,\xi_c)^{-\gamma} = \beta\,(1+g_c)^{-\gamma}(1-s_{t+1}\xi_c)^{-\gamma}. \tag{S5}$$

In the disaster case in $t+1$, consumption drops and therefore we discount that period's assets by less.

Housing services:

$$d_t = \delta H_t \tag{S6}$$

where δ is rental yield (or equivalent cash flow derived from housing value), and H_t is house value.

Note the disaster state affects housing prices through two distinct channels: ξ_h captures physical damage to housing stock, while ξ_c captures the broader consumption impact that affects valuation.

Housing asset pricing equation:

$$H_t = \begin{cases} \mathbb{E}_t \left[m_{t+1} (d_{t+1} + H_{t+1})(1 - s_{t+1}\xi_h) \right], & \text{If no disaster at } t \\ \mathbb{E}_t \left[m_{t+1} (d_{t+1} + H_{t+1})(1 - s_{t+1}\xi_h) \right] (1 - \xi_h), & \text{If disaster at } t \end{cases} \tag{S7}$$

or, collapsing and substituting $d_t = \delta H_t$

$$H_t = \mathbb{E}_t \left[m_{t+1} \, (1+\delta)(1 - s_{t+1} \, \xi_h) \, H_{t+1} \right] (1 - s_t \xi_h). \tag{S8}$$

When iterating forward, equation S7 becomes[1]

$$H_t = \mathbb{E}_t \left[\sum_{j=1}^{\infty} (1+\delta)^j \left(\prod_{k=1}^{j} m_{t+k} \, (1 - s_{t+k} \, \xi_h) \right) \right] (1 - s_t \xi_h). \tag{S9}$$

Mangroves reduce disaster losses to housing, but not to consumption

$$\xi_h^m = \xi_h (1 - a(d, w)), \tag{S10}$$

where ξ_h represents baseline property-level damage ratio in the absence of mangrove protection (equivalently denoted $\xi_h(\cdot, 0)$ when emphasizing the functional dependence on mangrove width), ξ_h^m is the damage ratio with mangrove protection, and $a(d, w)$ is the mangrove adaptation benefit for a property located d kilometers from mangroves of width w meters. The protection function satisfies $\partial a / \partial d < 0$ (protection decays with distance) and $\partial a / \partial w > 0$ (wider forests provide greater protection).

For the county-level representative property simulation, we use the distance-weighted average protection $\bar{a}(w)$ across flooded properties in each county. At the individual property level, protection varies with distance according to $a(d, w)$, but for computational tractability we simulate a representative property experiencing the county-mean protection benefit.

Critically, mangroves affect only housing damages (ξ_h), not consumption shocks (ξ_c). Disaster consumption shocks arise from income disruption, business closures, and evacuation costs—effects that occur regardless of structural damage to the home.

3.2. **Key Parameters.** This subsection documents the core parameters that govern preferences, discounting, housing-market dynamics, and disaster-related shocks in the model. For transparency and replicability, we report baseline values, symbols, and data sources (or standard calibrations) used throughout the quantitative exercises, and we indicate where assumptions are made. Table S1 summarizes all calibrated parameters used in our analysis.

[1]The disaster state s_{t+1} enters twice: once reducing physical payoffs via $(1 - s_{t+1}\xi_h)$ (cash flow effect), and once increasing the SDF via $(1 - s_{t+1}\xi_c)^{-\gamma}$ (discount rate effect).

TABLE S1. Baseline Parameter Calibration

Parameter	Symbol	Value	Source
Housing Market			
Rental yield	δ	7.0%	Florida market data (Table S2)
Preferences & Discounting			
Discount factor	β	0.95	Standard calibration
Risk aversion	γ	2.0	Consensus estimate[a]
Consumption growth	g_c	2.5%	US long-run average adjusted for Florida
Consumption Shocks			
RP10 consumption drop	ξ_c^{10}	1.0%	Conservative calibration[b]
RP25 consumption drop	ξ_c^{25}	2.0%	(see Section 3.2.3)
RP50 consumption drop	ξ_c^{50}	4.0%	
RP100 consumption drop	ξ_c^{100}	8.0%	
Storm Probabilities (Baseline)			
10-year event	p_{10}	10%	Annual exceedance probability
25-year event	p_{25}	4%	
50-year event	p_{50}	2%	
100-year event	p_{100}	1%	
Simulation			
Time horizon	T	77 years	2024–2100
Monte Carlo paths	N	1,000	

[a] Standard in consumption-based asset pricing literature; see Mehra and Prescott[38].
[b] Calibrated below developing economy estimates (7–11%) and comparable to Norwegian evidence with full insurance (3–5%); see main text Section 3.2.3.

3.2.1. *Storm occurrence probabilities.* We model hurricane occurrence using discrete storm categories based on return period (RP) thresholds. Rather than converting the Annual Exceedance Probabilities (AEP) into mutually exclusive severity bins, we utilize the marginal probabilities directly.

Standard exceedance probabilities. The return period definitions provide the following annual probabilities of equaling or exceeding a given intensity:

- RP_{10}: 10% probability ($P = 0.10$)
- RP_{25}: 4% probability ($P = 0.04$)
- RP_{50}: 2% probability ($P = 0.02$)
- RP_{100}: 1% probability ($P = 0.01$)

Independent storm draws. In each simulation year, we draw storm occurrences independently for each category using Bernoulli trials. This modeling choice reflects the fact that return periods measure intensity thresholds, not mutual exclusivity—a single year can experience multiple storm types. In the event that multiple storms occur within the same simulation year, the model applies the macroeconomic and structural damage shocks associated solely with the most severe storm drawn for that period.

3.2.2. *Climate change scenarios.* We model climate change through the hydrodynamic flood maps, which for the climate scenarios (S1CC and S2CC in our internal classification) are generated using future extreme sea levels under sea level rise. Extreme water levels are re-estimated

for mid-century conditions under the SSP5-8.5 scenario [20, 21], and the flood map for each return period is extracted from this future hazard distribution.

Crucially, this future hazard distribution already reflects that damaging water levels are reached more frequently under sea level rise. As the baseline sea level rises, the water level associated with each return period increases, so that a water level that is rare today (e.g., a present-day 100-year level) corresponds to a more frequent event in the future (a shorter return period). This redistribution of the hazard-probability curve is therefore embedded in the future flood maps: at each fixed return period, the future maps represent a more severe event than their present-day counterparts. For this reason, we hold the storm return-period probabilities *fixed* across the baseline and climate scenarios and apply no separate adjustment to storm frequency. Sampling storms at fixed return-period probabilities while applying the future flood maps captures the increased frequency of damaging conditions; applying an additional frequency scaling on top of this would double-count the effect already contained in the future hazard maps.

Climate change thus enters the damage calculation entirely through the future flood maps, in two ways:

Deeper inundation. Elevated water levels increase flood depths for properties that flood under both present-day and future conditions, raising the structural damage ratio ξ_h. As in the baseline, ξ_h is the mean ratio of structural damage to property value across all buildings that flood in a given county, scenario, and return period:

$$\xi_h^{\text{county, scenario, RP}} = \frac{1}{N_{\text{flooded}}^{\text{county, scenario, RP}}} \sum_{i \in \text{flooded}^{\text{county, scenario, RP}}} \frac{\text{damage}_i}{\text{value}_i}, \tag{S11}$$

computed conditional on flooding occurring, where the set of flooded properties N_{flooded} is determined separately for each county, return period, and climate scenario from the scenario-specific flood depths.

Expanded flood extent. Higher water levels also extend flooding into previously unaffected areas, so more properties flood under the climate scenario ($N_{\text{flooded}}^{\text{CC}} > N_{\text{flooded}}^{\text{baseline}}$). Because the flooded set is scenario-specific, this expansion carries through to the county-level aggregation, where the at-risk exposure base grows under climate change.

Both effects are generated within the same future hydrodynamic flood maps, so they are internally consistent: the maps describe the depth and extent of flooding for each return period under future sea levels, and the return-period probabilities are held unchanged between scenarios.

3.2.3. *Consumption shocks.* A critical parameter in our analysis is the consumption shock ξ_c that households experience when a hurricane strikes. While the rare disaster literature in asset pricing [39, 40, 36] calibrates consumption drops of 10–60% for macroeconomic catastrophes like the Great Depression or World War II, regional natural disasters produce substantially smaller consumption effects. Bakkensen and Barrage[41] show that even in the most vulnerable countries climate-related cyclone damages reduce consumption by 5% relative to the balanced growth path.

Empirical evidence from developing economies. To the best of our knowledge, the most comprehensive household-level evidence on consumption responses to tropical cyclones comes from developing countries. Anttila-Hughes and Hsiang[42] analyze typhoons in

the Philippines and find that household consumption declines by an average of 7.1%, with income falling by 6.6%. In India, Agarwal et al.[43] document an 11% consumption drop during the Chennai flood, with only 65% recovery thereafter. Similarly, Bui et al.[44] find that natural disasters in Vietnam reduce household income and expenditure by approximately 7%, with limited evidence of consumption smoothing. These large consumption responses reflect limited insurance coverage, constrained credit markets, and weak social safety nets in developing economies.

Evidence from advanced economies with direct consumption measurement. Espegren et al.[45] provide rare direct evidence on household consumption responses to natural disasters in an advanced economy. Using Norwegian administrative data linked to electronic transaction records, they exploit a unique institutional setting: universal natural disaster insurance that fully compensates direct property damages with minimal deductibles (approximately 2% of damages). Despite this comprehensive coverage, households in disaster-affected municipalities experience cumulative consumption declines of $1,460 over four years—representing 33% of direct damages. This consumption response substantially exceeds the concurrent income decline of $720 (16% of direct damages), with the gap driven primarily by steep falls in housing wealth (peak decline: $13,000 in year two). The consumption drop is concentrated among homeowners, consistent with estimated marginal propensities to consume out of housing wealth shocks of approximately 3% [46].

The Norwegian evidence establishes a critical benchmark for US hurricane calibration. Even with full insurance coverage eliminating direct property loss risk, indirect channels—particularly housing wealth effects—generate substantial consumption contractions. The 3–5% consumption decline observed in Norway over four years likely represents a *lower bound* for US hurricane impacts, for three reasons. First, US flood insurance coverage is far from universal, with take-up rates below 50% even in high-risk coastal areas [47], leaving many households exposed to uncompensated property losses. Second, federal disaster assistance, while substantial, covers only a fraction of uninsured losses [48]. Third, Norwegian disasters were primarily localized floods and landslides, whereas major US hurricanes like Katrina or Ian generate region-wide destruction simultaneously affecting labor markets, housing markets, and local amenities across entire metropolitan areas.

Limited direct consumption evidence from US hurricanes. Despite extensive study of US hurricane impacts on income and employment [49, 50], direct household consumption measurements remain limited in the literature. Existing studies consistently find that federal disaster assistance, insurance markets, and credit access enable substantial consumption smoothing [48, 51]. Deryugina et al.[49] document that Hurricane Katrina victims experienced only transitory income losses with full recovery within two years, suggesting effective smoothing of short-run income shocks.

However, the absence of consumption data leaves unresolved whether housing wealth effects documented by Espegren et al.[45]—which operated *despite* full insurance—similarly affect US hurricane victims. The Norwegian evidence suggests that even when direct property damages are fully compensated, indirect channels operating through housing wealth, local labor markets, and amenity values generate substantial consumption contractions. Given that US flood insurance coverage is substantially less comprehensive than Norway's universal scheme, and that major US hurricanes generate broader regional disruptions than the localized Norwegian events, actual US consumption effects may well exceed the Norwegian baseline of 3–5% over four years.

Calibration. Given this empirical evidence and substantial parameter uncertainty, we adopt a conservative calibration that reflects consumption smoothing mechanisms available in the United States while acknowledging the potential for significant consumption effects through housing wealth and regional disruption channels. We assign consumption shocks that increase with storm severity:

$$\xi_c = \begin{cases} 0.00 & \text{No storm} \\ 0.01 & \text{10-year return period} \\ 0.02 & \text{25-year return period} \\ 0.04 & \text{50-year return period} \\ 0.08 & \text{100-year return period} \end{cases} \tag{S12}$$

These values are positioned conservatively relative to all available empirical benchmarks:

- **Below developing country estimates** (7–11%): US households have greater access to credit, insurance, and federal disaster assistance than households in the Philippines, India, or Vietnam.
- **Spanning the Norwegian baseline** (3–5%): Our values range from 1% for moderate storms to 8% for catastrophic events. The lower end reflects that many US households have access to consumption smoothing mechanisms, while the upper end acknowledges that major hurricanes may exceed Norwegian disaster impacts due to incomplete insurance coverage and broader regional disruption.
- **Far below rare disaster benchmarks** (10–60%): Hurricane impacts remain regional and temporary, unlike macroeconomic catastrophes modeled in the rare disaster literature.

This calibration reflects: (1) extensive disaster relief infrastructure in the United States, including FEMA assistance for major hurricanes [48]; (2) widespread private insurance markets, though with significant coverage gaps in flood insurance; (3) household access to credit for consumption smoothing; and (4) the temporary and regional nature of hurricane impacts compared to macroeconomic disasters. Importantly, even this conservative calibration generates substantial present value differences between protected and unprotected properties through the state-dependent discount factor mechanism (Section 3.1.1), as the SDF amplifies the value of protection benefits that accrue in disaster states.

3.2.4. *Rental yield.* We impute implied rental yield using Bureau of Economic Analysis (BEA) personal consumption expenditures (PCE) data. Following equation S6 and Piazzesi et al. [35], the yield δ is effectively the housing services flow divided by housing stock value.

We compute the national housing share from BEA data as 16.67% ($3,603.6B housing PCE divided by $21,615.1B total PCE in 2024). Applying this share to Florida's total PCE of $1,463.5B yields an estimated $244.0B in Florida housing services. Combined with Florida's housing stock value of $3,500B (10.0M units at $350K median value), this yields:

$$\delta = \frac{\$244.0\text{B}}{\$3{,}500\text{B}} = 0.0697$$

Our Florida estimate of $\delta = 0.07$ is consistent with the Piazzesi et al. [35] framework. Although they do not report δ explicitly, their calibration implies a national rental yield. From Piazzesi et al. [35] Table 1, housing services represent 17.4% of total consumption expenditure. In their model, the housing expenditure share equals $\delta H/(\delta H + c)$ where c is non-housing consumption and H is housing value. Using their reported average housing value-to-consumption

ratio and expenditure share, this implies a national δ of approximately 5.0–5.5%. Our Florida estimate of 7.0% therefore represents a 1.5–2.0 percentage point premium over the national average, which we attribute to state-specific factors.

We validate our methodology using observed market price-to-rent ratios (the rental yield δ, defined as annual rent divided by property value) in major Florida metropolitan areas. For example, Miami's median rent of \$3,285/month and median home value of \$535,000 imply $\delta = 7.37\%$. Across the three Florida metro areas in Table S3, the yield averages 6.82%.

TABLE S2. Data Sources for Florida Rental Yield Calibration

Variable	**Source**	**Value**	**Year**
Florida Total PCE	FRED FLPCE[a]	\$1,463.5B	2024
National Housing & Utilities PCE	FRED DHUFRC1A027NBEA[b]	\$3,603.6B	2024
Florida Housing Units	Census ACS[c]	10.0M	2023
Florida Median Home Value	Market Data[d]	\$350K	2023–24
Housing Share (National)	BEA / Piazzesi[e]	16.67%	2024

[a] Federal Reserve Economic Data, https://fred.stlouisfed.org/series/FLPCE. Source: U.S. Bureau of Economic Analysis.

[b] Federal Reserve Economic Data, https://fred.stlouisfed.org/series/DHUFRC1A027NBEA. Personal consumption expenditures: Housing, utilities, and fuels.

[c] American Community Survey 2024 estimates, https://data.census.gov/profile/Florida?g=040XX00US12.

[d] Zillow Home Value Index, CoreLogic HPI, Miami Realtors monthly reports.

[e] BEA NIPA Table 2.5.5; validates Piazzesi et al. (2007) [35] estimate of 17.4%.

TABLE S3. Market-Based Rental Yield Estimates

Metro Area	**Median Rent**	**Median Home Value**	δ
Miami-Dade County	\$3,285/month[a]	\$535,000[d]	7.37%
Tampa-St. Petersburg	\$2,195/month[b]	\$390,000[e]	6.75%
Orlando	\$2,050/month[c]	\$387,500[f]	6.35%
Average			**6.82%**

Access Date: Feb 6, 2026.

To calculate the annualized rental yield (δ), we utilize publicly available Zillow market data from June 2024 for both median rents and home values. This timing captures stabilized market conditions at the onset of the Atlantic hurricane season, a period of high coastal risk salience.

While our core analysis focuses on seven coastal counties with significant mangrove coverage, we calibrate δ using major Florida metropolitan hubs (including inland Orlando) to reflect broader regional market dynamics.

[a] Zillow Rental Manager, Miami median rent, June 2024. https://www.zillow.com/rental-manager/market-trends/miami-fl/

[b] Zillow Rental Manager, Tampa median rent, June 2024. https://www.zillow.com/rental-manager/market-trends/tampa-fl/

[c] Zillow Rental Manager, Orlando median rent, June 2024. https://www.zillow.com/rental-manager/market-trends/orlando-fl/

[d] Zillow Home Value Index (ZHVI), Miami-Dade County, June 2024. https://www.zillow.com/home-values/2964/miami-dade-county-fl

[e] Zillow Home Value Index (ZHVI), Tampa, June 2024. https://www.zillow.com/home-values/41176/tampa-fl

[f] Zillow Home Value Index (ZHVI), Orlando, June 2024. https://www.zillow.com/home-values/13121/orlando-fl

3.2.5. *County-specific hedonic loss parameters.* Our market-based valuation uses the hedonic loss parameters from Liu et al. [4], which measure the effect of mangrove proximity on housing-price responses to hurricanes from a difference-in-differences design over more than one million transactions. In addition to the pooled statewide effect, that specification yields county-specific interaction estimates; we report them in Table S4. We use the county-specific parameter where it is consistent with a protective mechanism, and the pooled statewide estimate otherwise.

For Hillsborough, Manatee, Miami-Dade, and Pinellas, the county-specific estimates are correctly signed—near-mangrove properties experience smaller storm-related price declines—and statistically significant, and we use them directly (Table S4). For Charlotte, Collier, and Lee, the county-specific coefficients carry the opposite sign, implying that near-mangrove properties appreciate following storms; this is economically implausible for a flood-protection mechanism and most plausibly reflects county-specific confounders that a single-county subsample cannot separate from the protection effect (for example, waterfront amenity capitalization or post-storm redevelopment). For these three counties we therefore adopt the pooled statewide estimate ($\hat{\xi}_h^{100} = 0.074$), which is the well-identified average effect in Liu et al. [4].

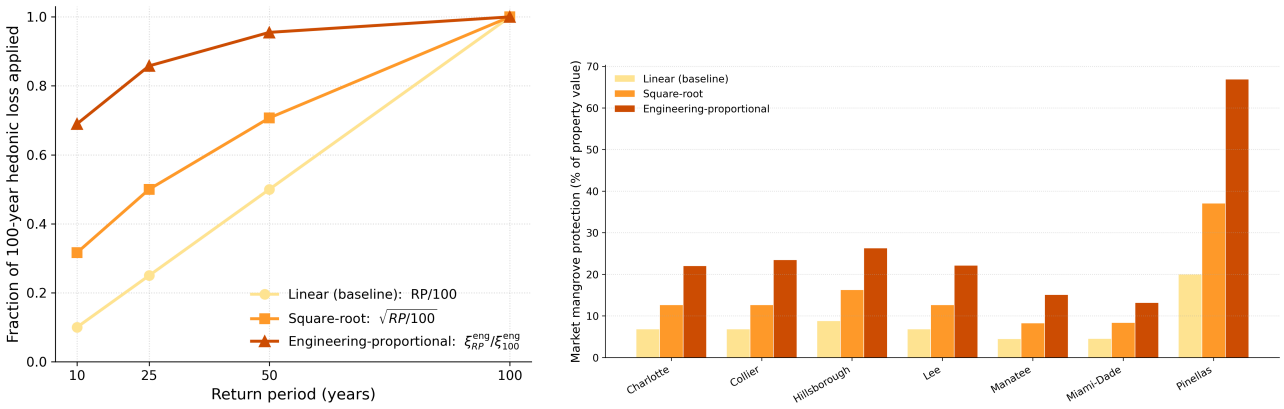
Relative to applying the pooled estimate to all counties, this refinement leaves the statewide comparison unchanged while modestly reallocating value across counties: the market-based mangrove value is slightly larger in Hillsborough, slightly smaller in Manatee and Miami-Dade, and substantially larger in Pinellas.

TABLE S4. Hedonic loss parameters used in the market-based valuation. Coefficients are the county × post-hurricane mangrove-proximity interactions from the headline specification in Liu et al. [4] (standard errors in parentheses); a negative interaction corresponds to mangrove flood protection. County-specific parameters are used where correctly signed; Charlotte, Collier, and Lee produced opposite-signed estimates and are assigned the pooled statewide estimate. Market value is mangrove protection as a percentage of property value in the baseline scenario (as shown in the main text of this paper).

County	Coef. (SE)	Parameter used	Market value (%)
Hillsborough	-0.065^{***} (0.007)	County-specific	8.8
Manatee	-0.036^{***} (0.009)	County-specific	4.5
Miami-Dade	-0.032^{***} (0.004)	County-specific	4.6
Pinellas	-0.116^{***} (0.007)	County-specific	20.0
Charlotte, Collier, Lee	opposite-signed	Pooled (0.074)	6.9

$^{***}p < 0.01$. The pooled statewide estimate is applied to counties whose county-specific interaction is not consistent with a protective sign.

3.2.6. *Sensitivity to the return-period scaling rule.* The hedonic loss parameter $\hat{\xi}_h$ is identified only for 100-year storms in [4], so we scale it to the shorter return periods. Our baseline applies a *linear* rule, $\hat{\xi}_h(\mathrm{RP}) = (\mathrm{RP}/100)\,\hat{\xi}_h^{100}$, reflecting the assumption that market-perceived losses scale in proportion to storm rarity. Because our results could in principle depend on this choice, we test two more aggressive alternatives: a *square-root* rule, $\hat{\xi}_h(\mathrm{RP}) = \sqrt{\mathrm{RP}/100}\,\hat{\xi}_h^{100}$, and an *engineering-proportional* rule that borrows the return-period shape of the engineering damage ratios, $\hat{\xi}_h(\mathrm{RP}) = (\xi_{\mathrm{RP}}^{\mathrm{eng}}/\xi_{100}^{\mathrm{eng}})\,\hat{\xi}_h^{100}$. Both alternatives assign more weight to frequent, smaller storms than the linear rule (Figure S3).



(A) (B)

FIGURE S3. Sensitivity of the market-based valuation to the return-period scaling rule. (a) Fraction of the 100-year hedonic loss applied at each return period under the linear (baseline), square-root, and engineering-proportional rules; both alternatives load more of the 100-year loss onto smaller, more frequent storms. (b) Resulting market-based mangrove protection value by county under each rule.

Figure S3 reports the resulting market-based mangrove protection value by county under each alternative, relative to the linear baseline. In every county, both alternatives *raise* the market estimate, confirming that the linear rule is the most conservative choice. Statewide, both the square-root and engineering-proportional rules substantially increase the market-based value and therefore further widen the already large gap between the market-based and avoided-damage estimates. Because every plausible alternative only increases the market estimate, one of our conclusions—that market-based values generally exceed avoided-damage values—is robust to, and if anything understated by, the choice of scaling rule.

3.3. **Comparing to hedonic measure.** To compare to the empirical results in Liu et al. [4], we consider only 100-year storms. Suppose a 100-year storm occurs at time t_0 but not in a previous year: $s_{t_0-1} = 0$, $s_{t_0} = 1$. We split the infinite sum in Equation S9 by pulling out the $j = 1$ term explicitly:

$$H_{t_0-1} = \mathbb{E}_{t_0-1}\left[(1+\delta)m_{t_0}(1-s_{t_0}\xi_h)\right] + \mathbb{E}_{t_0-1}\left[\sum_{j=2}^{\infty}(1+\delta)^j \prod_{k=1}^{j} m_{t_0-1+k}(1-s_{t_0-1+k}\xi_h)\right]$$

Re-indexing the second term with $j = i + 1$, the product from $k = 1$ to j splits into the t_0 factor times the product from $k = 1$ to i of post-t_0 terms:

$$H_{t_0-1} = \mathbb{E}_{t_0-1}\left[(1+\delta)m_{t_0}(1-s_{t_0}\xi_h)\left(1+\sum_{i=1}^{\infty}(1+\delta)^i \prod_{k=1}^{i} m_{t_0+k}(1-s_{t_0+k}\xi_h)\right)\right] \tag{S13}$$

Since storms are i.i.d. and m_{t_0+k} depends only on s_{t_0+k}, the post-t_0 continuation is measurable with respect to $\mathcal{F}_{t_0}$. By the law of iterated expectations $\mathbb{E}_{t_0-1}[\mathbb{E}_{t_0}[\cdot]] = \mathbb{E}_{t_0-1}[\cdot]$, we can write:

$$\Phi_{t_0} \equiv \mathbb{E}_{t_0}\left[\sum_{j=1}^{\infty}(1+\delta)^j \prod_{k=1}^{j} m_{t_0+k}(1-s_{t_0+k}\xi_h)\right] \tag{S14}$$

Since Φ_{t_0} is measurable at t_0, it is a constant with respect to $\mathbb{E}_{t_0-1}[\cdot]$ conditional on it being realized, giving:

$$H_{t_0-1} = \mathbb{E}_{t_0-1}\left[(1+\delta)m_{t_0}(1-s_{t_0}\xi_h)\right](1+\Phi_{t_0}) \tag{S15}$$

At t_0, the storm $s_{t_0} = 1$ is realized, so $(1 - s_{t_0}\xi_h) = (1 - \xi_h)$ is known and comes outside the expectation:

$$H_{t_0} = \Phi_{t_0}(1-\xi_h) \tag{S16}$$

Dividing H_{t_0} by H_{t_0-1}:

$$\frac{H_{t_0}}{H_{t_0-1}} = \frac{\Phi_{t_0}(1-\xi_h)}{\mathbb{E}_{t_0-1}\left[(1+\delta)m_{t_0}(1-s_{t_0}\xi_h)\right](1+\Phi_{t_0})} \tag{S17}$$

Since storms are i.i.d. and binary, taking value 1 with probability $\bar{p}$ and 0 otherwise, we have the continuation value given by a geometric series:

$$\Phi_{t_0} = \sum_{j=1}^{\infty}(1+\delta)^j\mu^j = \frac{(1+\delta)\mu}{1-(1+\delta)\mu}, \tag{S18}$$

so that $1 + \Phi_{t_0} = \dfrac{1}{1-(1+\delta)\mu}$, where $\mu \equiv \mathbb{E}[m(s)(1 - s\xi_h)]$ for periods after t_0.

Substituting into the ratio:

$$\frac{H_{t_0}}{H_{t_0-1}} = \frac{(1+\delta)\mu(1-\xi_h)}{\mathbb{E}_{t_0-1}\left[(1+\delta)m_{t_0}(1-s_{t_0}\xi_h)\right]} = \frac{\mu(1-\xi_h)}{\mathbb{E}_{t_0-1}\left[m_{t_0}(1-s_{t_0}\xi_h)\right]} \tag{S19}$$

which simplifies to $\frac{H_{t_0}}{H_{t_0-1}} = (1 - \xi_h)$ with full rational expectations.

3.4. **Comparison with the expected-damages valuation.** To isolate the contribution of the risk-based (catastrophic) asset-pricing framework, we compare our present-day catastrophic asset-pricing values with a conventional, risk-neutral expected-damages valuation computed from the same damage inputs and the same set of storms. For the expected-damages benchmark, we integrate the avoided-damage exceedance curve over only the four modeled return periods (10, 25, 50, and 100 years), with no extrapolation of damages below the 10-year storm, and discount the resulting annual expected benefit over 2024–2100 (77 years) at a constant 5% per year (Figure S4A). The catastrophic county totals (Figure S4B) are those reported in the main text, restricted to the same four return periods and shown on a common color scale. Because both approaches use identical damage inputs and identical storm coverage, the only difference between them is the valuation method.

With storm coverage held fixed, the catastrophic asset-pricing values exceed the expected-damages present value in every county. The difference reflects the risk adjustment that defines the asset-pricing framework: whereas the expected-damages calculation applies a constant discount rate to average losses, the catastrophic (risk-based) approach values each avoided loss through a stochastic discount factor that places greater weight on consumption in the high-marginal-utility states that follow storms. This state-dependent discounting adds a risk premium that a risk-neutral expected-damages valuation, by construction, omits. We note that the two approaches also differ in their effective discount rate—the asset-pricing model implies a risk-free rate above 5%—so the gap reflects the net of this higher base rate and the risk premium; that the catastrophic values are nonetheless larger indicates the risk premium dominates.

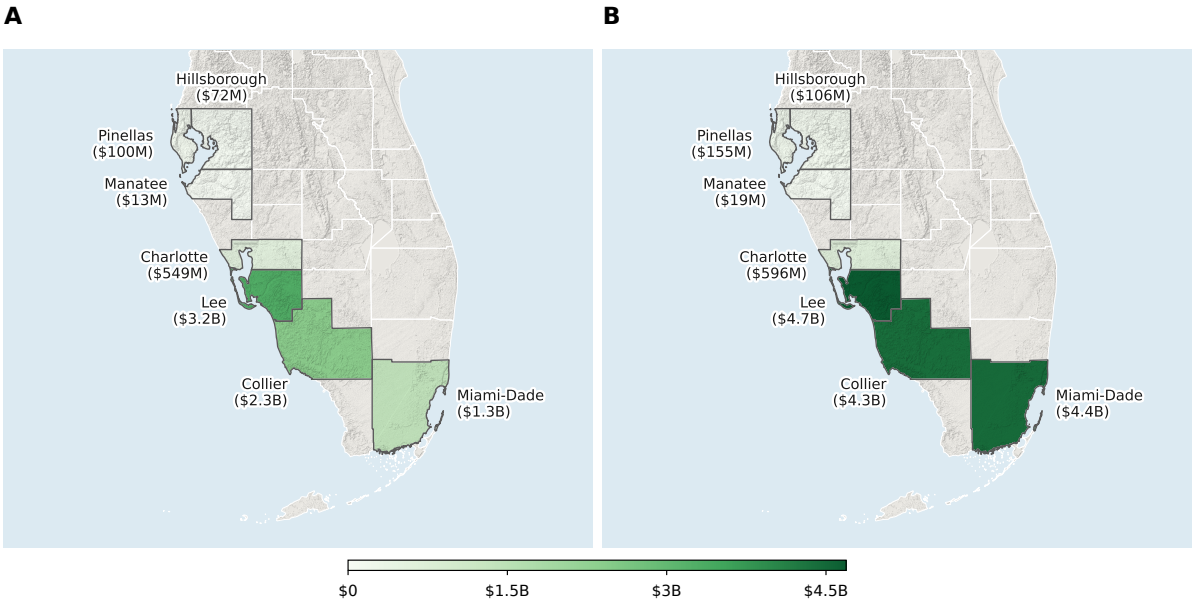


FIGURE S4. **Risk-based (catastrophic) asset pricing compared with expected damages.** Both panels use the four modeled return periods (10, 25, 50, and 100 years), with no extension of the damage curve below the 10-year storm. (A) Present value of the annual expected benefit of mangroves computed directly from expected damages under a risk-neutral, constant discount rate, over 2024–2100 (77 years) at 5% per year. (B) Risk-based (catastrophic) asset-pricing county totals using the same loss input under present climate, as in the main text. The catastrophic asset-pricing values exceed the expected-damages present value, reflecting the state-dependent discounting in the risk-based framework.

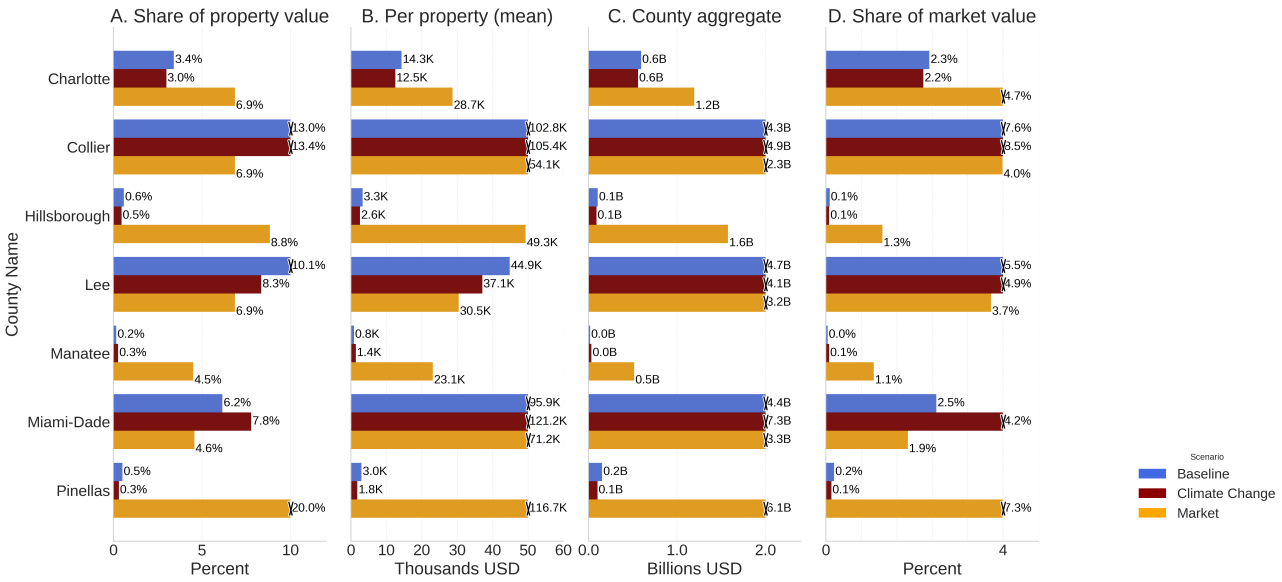


FIGURE S5. **Mangrove protection value by county** (unweighted loss parameter). A: share of property value; B: per-property mean (USD); C: county aggregate (USD); D: share of total housing (market) value. Baseline and climate-change bars use the risk-based (catastrophic) loss parameter; market bars use the hedonic loss parameter.

3.5. **County-level protection values.** The per-county values summarized in the main text are shown in full in Figure S5, across both dollar and normalized (share-of-value) metrics under the risk-based and market-based loss parameters.

Appendix A. Derivation of Eq. (S9)

This appendix derives the infinite-horizon sum–product representation in Eq. (S9) by forward-iterating the recursive pricing equation in Eq. (S8).

Let the pre-storm fundamental value of the asset be V_t. The recursive price-to-dividend equivalent is

$$V_t = \mathbb{E}_t \left[m_{t+1}(1+\delta)(1 - s_{t+1}\xi_h)(1+V_{t+1}) \right]. \tag{S20}$$

Distributing terms separates the next-period service flow from the continuation value:

$$V_t = \mathbb{E}_t \left[m_{t+1}(1+\delta)(1 - s_{t+1}\xi_h) + m_{t+1}(1+\delta)(1 - s_{t+1}\xi_h)V_{t+1} \right]. \tag{S21}$$

By recursion,

$$V_{t+1} = \mathbb{E}_{t+1} \left[m_{t+2}(1+\delta)(1 - s_{t+2}\xi_h)(1+V_{t+2}) \right]. \tag{S22}$$

Substituting into Eq. (S21) and applying the law of iterated expectations yields

$$V_t = \mathbb{E}_t \left[m_{t+1}(1+\delta)(1 - s_{t+1}\xi_h) + m_{t+1}m_{t+2}(1+\delta)^2(1 - s_{t+1}\xi_h)(1 - s_{t+2}\xi_h)(1+V_{t+2}) \right]. \tag{S23}$$

Iterating forward and imposing the standard transversality condition $\lim_{T\to\infty} \mathbb{E}_t[\dots V_{t+T}] = 0$ produces

$$V_t = \mathbb{E}_t \left[\sum_{j=1}^{\infty} (1+\delta)^j \left(\prod_{k=1}^{j} m_{t+k} \left(1 - s_{t+k}\, \xi_h\right) \right) \right]. \tag{S24}$$

Finally, the post-storm realized house value multiplies by the contemporaneous damage realization $(1 - s_t\xi_h)$,

$$H_t = \mathbb{E}_t \left[\sum_{j=1}^{\infty} (1+\delta)^j \left(\prod_{k=1}^{j} m_{t+k} \left(1 - s_{t+k}\, \xi_h\right) \right) \right] (1 - s_t\xi_h), \tag{S25}$$

which matches Eq. (S9).

Appendix B. Results obtained with structure value-weighted average loss ratio

As a robustness check, we recompute the county-level structural damage ratio ξ_h using an alternative aggregation method. Specifically, we recreate an earlier iteration of the engineering module in which the county-level loss ratio is computed as the ratio of mean damage to mean building value, rather than the mean of individual property-level loss ratios. Because high-value structures contribute more to both the numerator and denominator, this ratio-of-means approach effectively places greater weight on expensive properties. We then rerun the full pipeline—engineering-based damage estimation and the subsequent market/valuation assessment—using this alternative ξ_h. The purpose of this appendix is to verify that the estimated mangrove protection values are not highly sensitive to the choice of aggregation method and that the main qualitative conclusions remain unchanged.

Formally, the main-text aggregation in Equation S11 computes the unweighted mean of property-level loss ratios (mean-of-ratios). In contrast, the alternative aggregation computes the ratio of mean damage to mean value (ratio-of-means):

(S26)
$$\xi_{h,\,\text{ratio-of-means}}^{\text{county, scenario, RP}} = \frac{\frac{1}{N_{\text{flooded}}^{\text{county, scenario, RP}}} \sum_{i \in \text{flooded}^{\text{county, scenario, RP}}} \text{damage}_i}{\frac{1}{N_{\text{flooded}}^{\text{county, scenario, RP}}} \sum_{i \in \text{flooded}^{\text{county, scenario, RP}}} \text{value}_i} = \frac{\sum_{i \in \text{flooded}^{\text{county, scenario, RP}}} \text{damage}_i}{\sum_{i \in \text{flooded}^{\text{county, scenario, RP}}} \text{value}_i},$$

where $N_{\text{flooded}}^{\text{county, scenario, RP}}$ denotes the number of properties experiencing non-zero flood damage in the given county-scenario-return period cell, and the $1/N_{\text{flooded}}$ terms cancel. This ratio-of-means formulation is algebraically equivalent to a value-weighted average, as high-value properties contribute proportionally more to both total damage and total value.

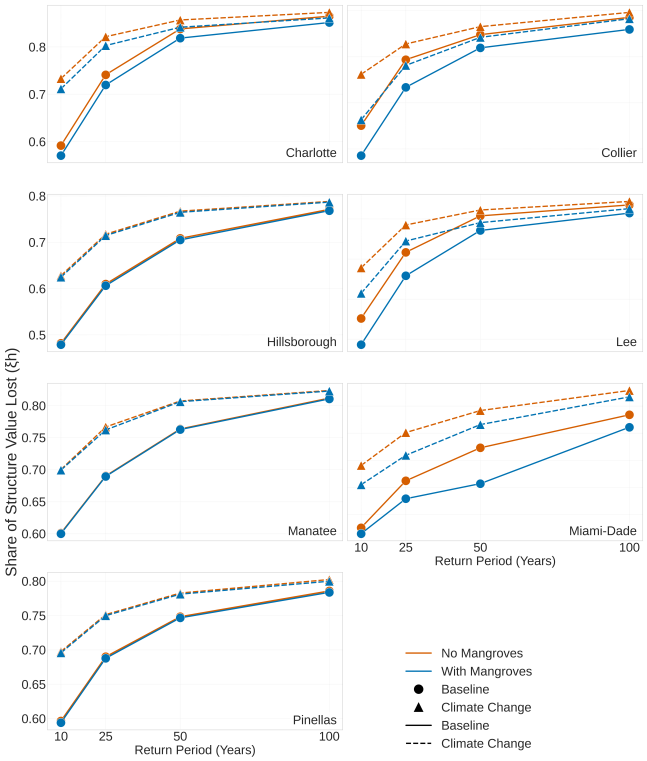


FIGURE S6. **Direct loss parameter (structure value-weighted).** Structure value-weighted average share of building value lost (ξ_h; ratio-of-means) among buildings affected by flooding, by county, return period, and scenario. For scenarios with mangrove protection, the loss parameter is probability-adjusted (multiplied by the ratio of buildings flooded with mangroves to those flooded without). This is the value-weighted counterpart to the unweighted (mean-of-ratios) direct loss parameter reported in the main text.

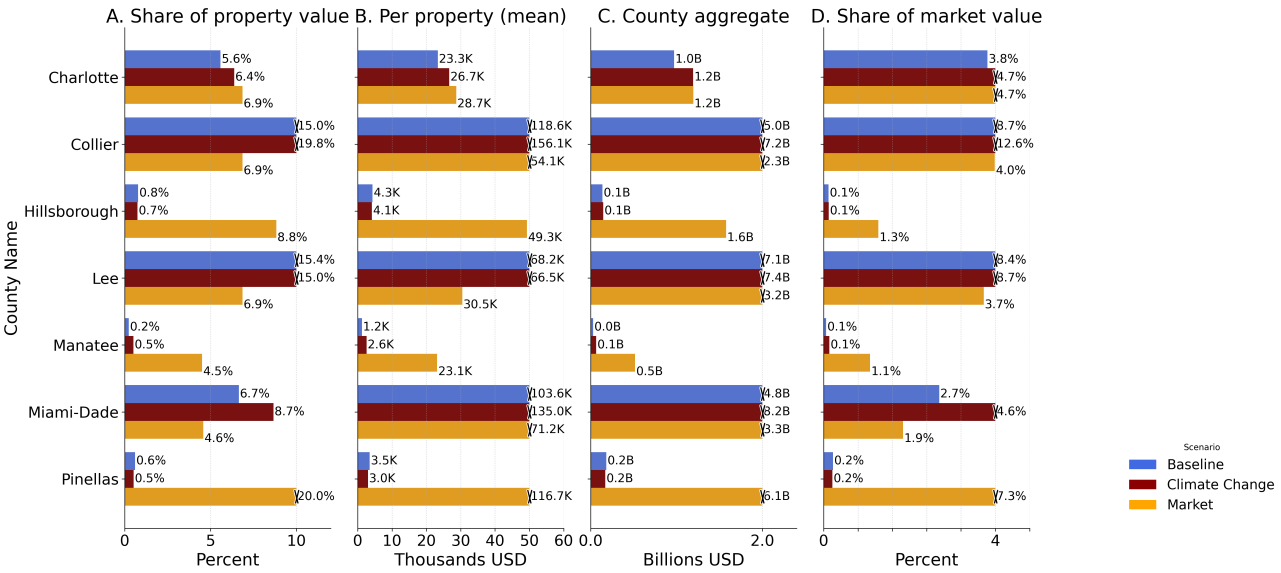


FIGURE S7. **Mangrove protection value by county** (structure value-weighted). A: share of property value; B: per-property mean (USD); C: county aggregate (USD); D: share of total housing (market) value. Baseline and climate-change bars use the risk-based (catastrophic) loss parameter; market bars use the hedonic loss parameter.

References

[1] Michael W. Beck, Nadine Heck, Siddharth Narayan, Pelayo Menéndez, Borja G. Reguero, Stephan Bitterwolf, Saul Torres-Ortega, Glenn-Marie Lange, Kerstin Pfliegner, Valerie Pietsch McNulty, and Iñigo J. Losada. Return on investment for mangrove and reef flood protection. *Ecosystem Services*, 56:101440, 2022.

[2] Siddharth Narayan, Christopher J. Thomas, Kechi Nzerem, Joss Matthewman, Christine Shepard, Laura Geselbracht, and Michael W. Beck. The spatially variable effects of mangroves on flood depths and losses from storm surges in Florida. *Cell Reports Sustainability*, 2(12):100531, 2025.

[3] Pelayo Menéndez, Iñigo J. Losada, Saul Torres-Ortega, Siddharth Narayan, and Michael W. Beck. The global flood protection benefits of mangroves. *Scientific Reports*, 10:4404, 2020.

[4] Teng Liu, Brook Constantz, Galina Hale, and Michael W Beck. Financial value of nature: coastal housing markets, mangroves, and climate resilience. *Review of Finance*, 30(1):87–129, 10 2026.

[5] Federal Emergency Management Agency. Flood Assessment Structure Tool (FAST). Technical manual, U.S. Department of Homeland Security, Federal Emergency Management Agency, 2024. Accessed: 2026.

[6] FEMA. Hazus flood model technical manual. Technical manual, Federal Emergency Management Agency, 2024.

[7] Tim Leijnse, Maarten van Ormondt, Kees Nederhoff, and Ap van Dongeren. Modeling compound flooding in coastal systems using a computationally efficient reduced-physics solver: The SFINCS model. *Coastal Engineering*, 163:103796, 2021.

[8] U.S. Geological Survey. 3D elevation program 1-meter resolution digital elevation model. The National Map, 2024.

[9] Cooperative Institute for Research in Environmental Sciences (CIRES). Continuously updated digital elevation model (CUDEM) — 1/9 arc-second resolution bathymetric-topographic tiles, 2014.

[10] Dean Gesch, Michael Oimoen, Susan Greenlee, Charles Nelson, Michael Steuck, and Dean Tyler. The national elevation dataset. *Photogrammetric Engineering and Remote Sensing*, 68(1):5–11, 2002.

[11] NOAA Office of Coast Survey. BlueTopo: A compilation of the nation's best available bathymetric data, 2024.

[12] NOAA National Centers for Environmental Information. ETOPO 2022 15 arc-second global relief model, 2022.

[13] U.S. Geological Survey. Annual NLCD collection 1 science products (ver. 1.2, june 2026), 2026.

[14] Pete Bunting, Ake Rosenqvist, Lammert Hilarides, Richard M. Lucas, Nathan Thomas, Takeo Tadono, Thomas A. Worthington, Mark Spalding, Nicholas J. Murray, and Lisa-Maria Rebelo. Global mangrove extent change 1996–2020: Global Mangrove Watch version 3.0. *Remote Sensing*, 14(15):3657, 2022.

[15] Alfred J. Kalyanapu, Steven J. Burian, and Timothy N. McPherson. Effect of land use-based surface roughness on hydrologic model output. *Journal of Spatial Hydrology*, 9(2):51–71, 2009.

[16] Keqi Zhang, Huiqing Liu, Yuepeng Li, Hongzhou Xu, Jian Shen, Jamie Rhome, and Thomas J. Smith. The role of mangroves in attenuating storm surges. *Estuarine, Coastal and Shelf Science*, 102–103:11–23, 2012.

[17] Job C. M. Dullaart, Sanne Muis, Nadia Bloemendaal, Maria V. Chertova, Anaïs Couasnon, and Jeroen C. J. H. Aerts. Accounting for tropical cyclones more than doubles the global population exposed to low-probability coastal flooding. *Communications Earth & Environment*, 2:135, 2021.

[18] Nadia Bloemendaal, Ivan D. Haigh, Hans de Moel, Sanne Muis, Reindert J. Haarsma, and Jeroen C. J. H. Aerts. Generation of a global synthetic tropical cyclone hazard dataset using storm. *Scientific Data*, 7(1):40, Feb 2020.

[19] Hans Hersbach, Bill Bell, Paul Berrisford, Shoji Hirahara, András Horányi, Joaquín Muñoz-Sabater, Julien Nicolas, Carole Peubey, Raluca Radu, Dinand Schepers, Adrian Simmons, Cornel Soci, Saleh Abdalla, Xavier Abellan, Gianpaolo Balsamo, Peter Bechtold, Gionata Biavati, Jean Bidlot, Massimo Bonavita, Giovanna De Chiara, Per Dahlgren, Dick Dee, Michail Diamantakis, Rossana Dragani, Johannes Flemming, Richard Forbes, Manuel Fuentes, Alan Geer, Leopold Haimberger, Sean Healy, Robin J. Hogan, Elías Hólm, Marta Janisková, Sarah Keeley, Patrick Laloyaux, Philippe Lopez, Cristina Lupu, Gabor Radnoti, Patricia de Rosnay, Iryna Rozum, Freja Vamborg, Sebastien Villaume, and Jean-Noël Thépaut. The ERA5 global reanalysis. *Quarterly Journal of the Royal Meteorological Society*, 146(730):1999–2049, 2020.

[20] Li H. Erikson, Liv Herdman, Christie Flanary, Anita C. Engelstad, Pavithra Pusuluri, Patrick L. Barnard, Curt D. Storlazzi, Michael W. Beck, Borja G. Reguero, and Kees A. Parker. Ocean wave time-series data simulated with a global-scale numerical wave model under the influence of projected CMIP6 wind and sea ice fields. U.S. Geological Survey, Santa Cruz, CA [Data product], 2023.

[21] Sanne Muis, Maialen Irazoqui Apecechea, José A. Álvarez, Martin Verlaan, Kun Yan, Job Dullaart, Jeroen Aerts, Trang Duong, Roshanka Ranasinghe, Dewi le Bars, Reindert Haarsma, and Malcolm Roberts. Global sea level change time series from 1950 to 2050 derived from reanalysis and high resolution CMIP6 climate projections. Copernicus Climate Change Service (C3S) Climate Data Store (CDS) [Data set], 2022.

[22] J. C. M. Dullaart, S. Muis, H. de Moel, P. J. Ward, D. Eilander, and J. C. J. H. Aerts. Enabling dynamic modelling of coastal flooding by defining storm tide hydrographs. *Natural Hazards and Earth System Sciences*, 23(5):1847–1862, 2023.

[23] IPCC. Climate change 2023: Synthesis report. contribution of working groups I, II and III to the sixth assessment report of the intergovernmental panel on climate change. Technical report, Intergovernmental Panel on Climate Change, Geneva, Switzerland, 2023. Core Writing Team, H. Lee and J. Romero (eds.).

[24] U.S. Army Corps of Engineers. National Structure Inventory (nsi) 2022, 2022. Hydrologic Engineering Center.

[25] Microsoft. Microsoft Open Buildings: Global building footprints dataset, 2024. Data set.

[26] U.S. Bureau of Labor Statistics. CPI Inflation Calculator, 2025. Consumer Price Index.

[27] Charles Scawthorn, Neil Blais, Hope Seligson, Eric Tate, Edward Mifflin, Will Thomas, James Murphy, and Christopher Jones. HAZUS-MH Flood Loss Estimation Methodology. I: Overview and Flood Hazard Characterization. *Natural Hazards Review*, 7(2):60–71, 2006.

[28] Charles Scawthorn, Paul Flores, Neil Blais, Hope Seligson, Eric Tate, Stephanie Chang, Edward Mifflin, Will Thomas, James Murphy, Christopher Jones, and Michael Lawrence. HAZUS-MH Flood Loss Estimation Methodology. II: Damage and Loss Assessment. *Natural Hazards Review*, 7(2):72–81, 2006.

[29] Borja G. Reguero, Michael W. Beck, David N. Bresch, Juliano Calil, and Imen Meliane. Comparing the cost effectiveness of nature-based and coastal adaptation: A case study from the Gulf Coast of the United States. *PLoS ONE*, 13(4):e0192132, 2018.

[30] Borja G. Reguero, Curt D. Storlazzi, Ann E. Gibbs, James B. Shope, Aaron D. Cole, Kristen A. Cumming, and Michael W. Beck. The value of US coral reefs for flood risk reduction. *Nature Sustainability*, 4:688–698, 2021.

[31] Rae Taylor-Burns, Christopher Lowrie, Babak Tehranirad, Jennifer Lowe, Li Erikson, Patrick L. Barnard, Borja G. Reguero, and Michael W. Beck. The value of marsh restoration for flood risk reduction in an urban estuary. *Scientific Reports*, 14:6856, 2024.

[32] Herbert E. Gene Longenecker, III. Development and applications of the fema region iv coastal flood loss atlas. In *Solutions to Coastal Disasters 2011*, pages 650–665. American Society of Civil Engineers, 2011.

[33] Florida Office of Broadband. Florida county boundaries. https://florida-office-of-broadband-flbroadband.hub.arcgis.com/datasets/florida-county-boundaries/explore, March 2024. Data set, 67 records. Published 25 March 2024; data last updated 12 May 2025. Accessed 20 January 2026.

[34] Thomas A. Rietz. The equity risk premium: A solution. *Journal of Monetary Economics*, 22(1):117–131, 1988.

[35] Monika Piazzesi, Martin Schneider, and Selale Tuzel. Housing, consumption and asset pricing. *Journal of Financial Economics*, 83(3):531–569, 2007.

[36] Xavier Gabaix. Variable rare disasters: An exactly solved framework for ten puzzles in macro-finance. *The Quarterly Journal of Economics*, 127(2):645–700, 2012.

[37] Jessica A. Wachter. Can time-varying risk of rare disasters explain aggregate stock market volatility? *Journal of Finance*, 68(3):987–1035, 2013.

[38] Rajnish Mehra and Edward C Prescott. The equity premium: A puzzle. *Journal of Monetary Economics*, 15(2):145–161, 1985.

[39] Robert J Barro. Rare disasters and asset markets in the twentieth century. *The Quarterly Journal of Economics*, 121(3):823–866, 2006.

[40] Robert J Barro. Rare disasters, asset prices, and welfare costs. *American Economic Review*, 99(1):243–64, 2009.

[41] Laura A. Bakkensen and Lint Barrage. Climate shocks, cyclones, and economic growth: Bridging the micro-macro gap. *The Economic Journal*, 136(673):279–310, 2026.

[42] Jesse K Anttila-Hughes and Solomon M Hsiang. Destruction, disinvestment, and death: Economic and human losses following environmental disaster. *Available at SSRN 2220501*, 2013.

[43] Sumit Agarwal, Pulak Ghosh, and Huanhuan Zheng. Consumption response to a natural disaster: Evidence of price and income shocks from chennai flood. *Energy Economics*, 131:107323, 2024.

[44] Anh Tuan Bui, Mardi Dungey, Cuong Viet Nguyen, and Thu Phuong Pham. The impact of natural disasters on household income, expenditure, poverty and inequality: evidence from vietnam. *Applied Economics*, 46(15):1751–1766, May 2014.

[45] Caroline Espegren, Sigurd Mølster Galaasen, Emilia Garcia-Appendini, and Mathis Mæhlum. Weathering the storm? the effects of natural disasters on households under universal insurance. Technical report, 2025. Working paper presented at the NHH Department of Business and Management Science Seminar.

[46] Adam M Guren, Alisdair McKay, Emi Nakamura, and Jón Steinsson. Housing wealth effects: The long view. *Review of Economic Studies*, 88(2):669–707, 2021.

[47] Carolyn Kousky. The role of natural disaster insurance in recovery and risk reduction. *Annual Review of Resource Economics*, 10:541–561, 2018.

[48] Tatyana Deryugina. The fiscal cost of hurricanes: Disaster aid versus social insurance. *American Economic Journal: Economic Policy*, 9(3):168–98, 2017.

[49] Tatyana Deryugina, Laura Kawano, and Steven Levitt. The economic impact of hurricane katrina on its victims: Evidence from individual tax returns. *American Economic Journal: Applied Economics*, 10(2):202–33, 2018.

[50] Brigitte Roth Tran and Daniel J. Wilson. The local economic impact of natural disasters. *Journal of the Association of Environmental and Resource Economists*, 12(6):1667–1704, 2025.

[51] Justin Gallagher and Daniel Hartley. Household finance after a natural disaster: The case of hurricane katrina. *American Economic Journal: Economic Policy*, 9(3):199–228, 2017.